Theor Chim Acta (1991) 80: 307–319

Theoretica Chimica Acta

Application of the coupled-cluster theory to atomic frequency-dependent polarizabilities

Z. W. Liu and H. P. Kelly
Department of Physics, University of Virginia, Charlottesville, VA 22901, USA

Received February 1, 1991; received in revised form March 10, 1991/Accepted March 20, 1991

Summary. A time-dependent coupled-cluster approach may be employed to describe dynamic processes of many-electron systems. Atomic properties, such as the frequency-dependent polarizability, can be treated as a response of the system described by the coupled-cluster expansion to an external radiation field. The major difficulty in the realization of such a formalism is to deal with dynamic pair functions. The procedure reported here is to simplify the full set of single- and pair-excitation expansion equations to a subset of equations which includes polarization and relaxation effects to all orders and is solved by using a complete set of discrete basis functions. Calculations of excitation energies and frequency-dependent electric dipole polarizabilities for helium are presented. Application of the procedure to calculate photoionization cross sections is discussed.

Key words: Many-body perturbation theory – Coupled-cluster approach – Frequency-dependent polarizabilities – Atomic helium

1. Introduction

Correlation effects of a many-electron system subjected to a time-dependent external interaction may be studied by the time-dependent coupled-cluster (TDCC) approach [1–4], which is the application of the coupled-cluster theory [5–7] to dynamic processes of atoms and molecules. TDCC is equivalent to summation of large numbers of Goldstone diagrams corresponding to a certain truncation level of multiple-particle excitations and with some electron-electron lines replaced by external perturbation lines. The TDCC formalism, as reported by several groups [1–4], provides a useful method to calculate not only dynamic but also static properties of atoms and molecules, such as excitation energies, transition probabilities, and frequency-dependent polarizabilities. To our knowledge, however, there are no published results thus far of the implementation of this formalism. The major difficulty encountered in implementing the formalism in dealing with the dynamic pair functions.

The procedure presented in this work is to simplify the full set of single-particle and pair excitation amplitude equations to a subset of equations to take

account of polarization and relaxation effects to all orders. As is well known, the truncation scheme including only single-particle excitation amplitudes in the TDCC formalism leads to the Tamm–Dancoff approximation (TDA) [8]. When complex-conjugated single-particle excitation amplitudes are also considered, one can obtain the random-phase approximation (RPA) [9–10]. From the point of view of many-body perturbation theory (MBPT), the RPA results correspond to the first-order correlation corrections together with their higher-order chains, i.e. contributions obtained by iterating the first-order corrections. In this work the all-order polarization and relaxation approximation (PRA) scheme gives a prescription for iterating not only first-order corrections, but also those second-order corrections obtained by coupling pair excitations with single-particle excitations. Significant improvement of accuracy in the present PRA scheme is expected.

Many-body perturbation theory (MBPT) provides a systematic approach to obtain high-accuracy results for atomic properties. One of the advantages of MBPT is to use diagrammatic representation to give a clear interpretation of the physics behind calculations. However, the major disadvantage of MBPT is that the inclusion of higher-order diagrams can be very tedious and time consuming. The present method has the advantage of MBPT in showing a clear picture of what kind of correction effects are included in the calculation, and also includes higher-order terms of MBPT by summing certain classes of diagrams to all orders.

In Sect. 2 we give a brief outline of the TDCC theory for dynamic polarizability calculations. In Sect. 3 we derive the all-order PRA scheme as a reasonable approximation for the CCSD in dynamic processes. Following this derivation, in Sect. 4 we apply the PRA method to helium by using a finite-basis-set expansion in the relativistic frame work. Therefore, the method implemented in our work can be applied to heavy atoms.

2. Time-dependent coupled-cluster theory

The TDCC theory [1–4] is applied to an N-electron atom with the Dirac–Coulomb Hamiltonian plus an additional interaction term:

$$H = H_0 + H_c + V'(t), \tag{1}$$

where

$$H_0 = \sum_i [c\alpha_1 \cdot p_i + m(\beta_i - 1)c^2 + V_{\text{nuc}}(r_i) + U(r_i)], \tag{2}$$

and

$$H_c = \sum_{i<j}^{N} v_{ij} - \sum_i^N U(r_i). \tag{3}$$

The term $V_{\text{nuc}}(r_i)$ is the nuclear potential, $U(r_i)$ is an independent-particle-model potential, and v_{ij} represents the Coulomb interaction between pairs of electrons. When the atom is exposed to an external electromagnetic field, the additional time-dependent interaction $V'(t)$ is given as:

$$V'(t) = \sum_i [V_+(\boldsymbol{r}_i)\, e^{-i\omega t} + V_-(\boldsymbol{r}_i)\, e^{i\omega t}]\, e^{-\alpha|t|}, \tag{4}$$

where the time-independent operators $V_{\pm}(r)$ may be expressed as a multipole expansion of scalar and vector potentials of the radiation field [11] and satisfy $V_{+} = V_{-}^{*}$ to ensure Hermiticity of $V'(t)$, $e^{-\alpha|t|}$ is an adiabatic-switching factor.

The solution $\Psi(t)$ of the time-dependent Schrödinger equation:

$$i\frac{\partial}{\partial t}\Psi(t) = H\Psi(t) \tag{5}$$

may be written as the form [1–4] of:

$$\Psi(t) = e^{-iEt - i\varepsilon(t)}\Omega'(t)\Omega\Phi_0. \tag{6}$$

It implies a two-step procedure to solve Eq. (5) for $\Psi(t)$. At the first step, we solve a time-independent Schrödinger equation of:

$$(H_0 + H_c)\Omega\Phi_0 = E\Omega\Phi_0 \tag{7}$$

for the wave operator Ω with a coupled-cluster exponential ansatz [5–7]:

$$\Omega = \exp\{S\}, \tag{8}$$

where $\{S\}$ is the normal-ordered correlation operator S, and the unperturbed state Φ_0 satisfies:

$$H_0\Phi_0 = E_0\Phi_0. \tag{9}$$

Then, substituting Eq. (6) into Eq. (5), we can go further to solve for the time-dependent wave operator $\Omega'(t) = \exp\{T(t)\}$ and the level-shift phase factor $\varepsilon(t)$:

$$\left[E + \frac{d\varepsilon(t)}{dt}\right]\Omega'(t)\Omega\Phi_0 + i\frac{d\Omega'(t)}{dt}\Omega\Phi_0 = [H_0 + H_c + V'(t)]\Omega'(t)\Omega\Phi_0 \tag{10}$$

with initial conditions:

$$\lim_{t\to-\infty}\Omega'(t) = 1, \qquad \lim_{t\to-\infty}\varepsilon(t) = 0. \tag{11}$$

Without losing generality, we can take a linearized coupled-cluster expansion:

$$\Omega'(t)\Omega = \exp\{T(t)\}\exp\{S\} \approx 1 + S + T(t) \tag{12}$$

to show the derivation of working equations, and consider that the linearization of the equation takes place after cancellation of unlinked diagrams. Remaining non-linear terms can be included in the formalism later if desired.

By using a projection operator $P = |\Phi_0\rangle\langle\Phi_0|$ and its complement operator $Q = 1 - P$, we extend the generalized Bloch-equation [6] to a time-dependent form for the excitation amplitude $T(t)$ and parameter $\varepsilon(t)$ as:

$$[T, H_0]|\Phi_0\rangle + i\frac{dT}{dt}|\Phi_0\rangle = \{QV'(1 + S + T) + QH_cT - SP[H_cT + V'(1+S+T)] - TP[(H_c + V')(1 + S + T)]\}_{\text{linked}}|\Phi_0\rangle \tag{13}$$

and

$$\frac{d\varepsilon}{dt} = \langle\Psi_0|V'(1 + S + T)|\Phi_0\rangle/\langle\Psi_0|\Psi_0\rangle_v, \tag{14}$$

where $|\Psi_0\rangle = \Omega|\Phi_0\rangle$, and the subscript "$v$" for the normalization term indicates that only valence normalization terms remain after cancellation of unlinked

terms [12]. Then we introduce a perturbation expansion for $T(t)$ and $\varepsilon(t)$ in terms of multiphoton interactions as:

$$T(t) = \sum_{n=1} T^{(n)}(t), \tag{15}$$

$$\varepsilon(t) = \sum_{n=1} \varepsilon^{(n)}(t), \tag{16}$$

and $T^{(0)}(t) = 0$, $\varepsilon^{(0)}(t) = 0$. In the order of n-photon interactions, we obtain:

$$\begin{aligned}
&[T^{(n)}, H_0]|\Phi_0\rangle + i\frac{dT^{(n)}}{dt}|\Phi_0\rangle \\
&\quad = \{\delta_{n1} QV'(1+S) + QV'T^{(n-1)} + QH_cT^{(n)} \\
&\qquad - SP[H_cT^{(n)} + \delta_{n1} V'(1+S) + V'T^{(n-1)}] \\
&\qquad - T^{(n)}PH_c(1+S) - T^{(n-1)}PV'(1+S) \\
&\qquad - \sum_{m=1}^{n-1} T^{(m)}P[H_cT^{(n-m)} + V'T^{(n-m-1)}]\}_{\text{linked}}|\Phi_0\rangle
\end{aligned} \tag{17}$$

and

$$\frac{d\varepsilon^{(n)}}{dt} = \langle\Psi_0|[\delta_{n1} V'(1+S) + V'T^{(n-1)}]|\Phi_0\rangle / \langle\Psi_0|\Psi_0\rangle_v. \tag{18}$$

The simplest case of the solution of Eqs. (17–18) is to consider a dipole approximation with one photon interaction, i.e.:

$$V_+(\boldsymbol{r}) = \tfrac{1}{2}\hat{\boldsymbol{e}} \cdot \boldsymbol{r} = V_-^*(\boldsymbol{r}), \tag{19}$$

and $\hat{\boldsymbol{e}}$ is the polarization vector of the external electromagnetic field. Then Eqs. (17–18) lead to:

$$\begin{aligned}
&[T^{(1)}, H_0]|\Phi_0\rangle + i\frac{dT^{(1)}}{dt}|\Phi_0\rangle \\
&\quad = \{QV'(1+S) + QH_cT^{(1)} - T^{(1)}PH_c(1+S)\}_{\text{linked}}|\Phi_0\rangle,
\end{aligned} \tag{20}$$

$$\varepsilon^{(1)} = 0, \tag{21}$$

and

$$\frac{d\varepsilon^{(2)}}{dt} = \langle\Psi_0|V'T^{(1)}|\Phi_0\rangle / \langle\Psi_0|\Psi_0\rangle_v, \tag{22}$$

where the parity selection rule for dipole approximation has been considered. The linear response function $T^{(1)}$ consists of positive-frequency and negative-frequency parts:

$$T^{(1)} = T^{+1}\, e^{-i\omega t} + T^{-1}\, e^{i\omega t}, \tag{23}$$

where $T^{\pm 1}$ satisfy:

$$\begin{aligned}
&[T^{\pm 1}, H_0]|\Phi_0\rangle \pm \omega T^{\pm 1}|\Phi_0\rangle \\
&\quad = \{QV_\pm(1+S) + QH_cT^{\pm 1} - T^{\pm 1}PH_c(1+S)\}_{\text{linked}}|\Phi_0\rangle.
\end{aligned} \tag{24}$$

The solution of Eq. (22) contributes to the time-averaged second-order energy correction:

$$\bar{E}^{(2)}(\omega) = \frac{\omega}{2\pi}\int_0^{2\pi/\omega} \frac{d\mathcal{E}^{(2)}(t)}{dt}\,dt = -\tfrac{1}{2}\alpha(\omega), \tag{25}$$

where $\alpha(\omega)$ is the frequency-dependent polarizability:

$$\alpha(\omega) = -2\langle\Psi_0|V_+ T^{-1} + V_- T^{+1}|\Phi_0\rangle/\langle\Psi_0|\Psi_0\rangle_v, \tag{26}$$

which describes the linear response of the electron distribution to an external electric field and is directly related to dielectric constants, indices of refraction, photoionization cross sections and other important atomic parameters in dynamic processes [13]. The expression of Eq. (26) is connected with the polarization propagator method [14], as discussed in Ref. [4].

3. All-order polarization and relaxation approximation scheme

In this section we start with a standard linearized coupled-cluster singles and doubles (CCSD) expansion for the conventional wave operator Ω [5–7] and the time-dependent wave operator $\Omega(t)$ [1–4], and then we simplify the procedure to the PRA scheme.

By invoking second quantization, the perturbation interaction terms in Eq. (1) are written in normal order with respect to the core state as:

$$H_c = V_0 + V_1 + V_2, \tag{27}$$

where

$$V_0 = -\sum_a U_{aa} + \tfrac{1}{2}\sum_a (V_{HF})_{aa}, \tag{28}$$

$$V_1 = \sum_{ij} \Delta_{ij}\{a_i^+ a_j\}, \tag{29}$$

$$V_2 = \tfrac{1}{2}\sum_{ijkl} g_{ijkl}\{a_i^+ a_j^+ a_l a_k\}, \tag{30}$$

and

$$V' = \sum_{ij} V'_{ij}\{a_i^+ a_j\}, \tag{31}$$

where the operators inside the curl $\{\cdots\}$ are arranged in normal order with respect to core, g_{ijkl} are the Coulomb integrals, and:

$$\Delta_{ij} = (V_{HF})_{ij} - U_{ij}. \tag{32}$$

We use subscripts, a, b, c, d to denote occupied core orbitals, subscripts r, s, t, u to represent unoccupied excited states, and subscripts i, j, k, l to designate arbitrary states. The correlation operators truncated up to pair-excitation terms can be expressed by:

$$S \approx S_1 + S_2, \qquad T \approx T_1 + T_2 \tag{33}$$

where

$$S_1|\Phi_0\rangle = \sum_{ra} S_{ra} a_r^+ a_a |\Phi_0\rangle, \tag{34}$$

$$S_2|\Phi_0\rangle = \tfrac{1}{2} \sum_{rsab} S_{rsab} a_r^+ a_s^+ a_b a_a |\Phi_0\rangle, \tag{35}$$

and

$$T_1^{\pm}|\Phi_0\rangle = \sum_{ra} T_{ra}^{\pm} a_r^+ a_a |\Phi_0\rangle, \tag{36}$$

$$T_2^{\pm}|\Phi_0\rangle = \tfrac{1}{2} \sum_{rsab} T_{rsab}^{\pm} a_r^+ a_s^+ a_b a_a |\Phi_0\rangle. \tag{37}$$

Equations (34–37) include only terms for closed-shell atoms, but they may be extended to open-shell atoms [6, 12]. This is why we keep the terms corresponding to folded diagrams in Eqs. (13) and (14).

Substituting Eqs. (27–37) into Eq. (24), we obtain a set of equations for amplitudes $T_1^{\pm}$ and $T_2^{\pm}$ which depend on frequencies ω. These equations may be written in matrix form as:

$$\begin{pmatrix} A & B \\ C & C \end{pmatrix} \begin{pmatrix} T_1^{\pm} \\ T_2^{\pm} \end{pmatrix} = \mp\omega \begin{pmatrix} T_1^{\pm} \\ T_2^{\pm} \end{pmatrix} + \begin{pmatrix} R_1 \\ R_2 \end{pmatrix}, \tag{38}$$

where A, B, C, D are matrices constructed by Coulomb integrals, and R_1, R_2 are column vectors containing driving terms from the external field. The formalism of Eq. (38) has been previously discussed by Monkhorst [1], Mukherjee and Mukherjee [2], Sekino and Bartlett [3], Dalgaard and Monkhorst [4]. Because the dimension of $T_2^{\pm}$ amplitudes is huge, to really solve Eq. (38) is very demanding. However, by observing that the diagonal terms in Eq. (38) are dominant and the major driving terms come from R_1, we can greatly simplify it. The explicit expression of Eq. (38) is:

$$A_{ii}(T_1^{\pm})_i + \sum_{j=1\ (i\neq j)}^{n} A_{ij}(T_1^{\pm})_j + \sum_{l=1}^{m} B_{il}(T_2^{\pm})_l = \mp\omega(T_1^{\pm})_i + (R_1)_i \quad i = 1, 2, \ldots, n \tag{39}$$

$$\sum_{j=1}^{n} C_{kj}(T_1^{\pm})_j + \sum_{l=1\ (k\neq 1)}^{m} D_{kl}(T_2^{\pm})_l + D_{kk}(T_2^{\pm})_k = \mp\omega(T_2^{\pm})_k + (R_2)_k \quad k = 1, 2, \ldots, m, \tag{40}$$

where n and m is the dimension of the single- and pair-excitation amplitudes, respectively. We multiply the k-th equation of Eq. (40) with $(T_1^{\pm})_i$ and subtract it from the i-th equation of Eq. (39) multiplied with $(T_2^{\pm})_k$ to eliminate the terms with ω, then we find:

$$(T_2^{\pm})_k \approx -\frac{\sum_{j=1}^{n} C_{kj}(T_1^{\pm})_j - (R_2)_k}{D_{kk} - A_{ii}} \tag{41}$$

for the i-th Eq. (39) with the diagonal term A_{ii}. In derivation of Eq. (41), all terms including products of $(T_2^{\pm})_k$ with non-diagonal matrix elements are neglected. Substituting Eq. (41) into Eq. (39), we obtain:

$$A'T_1^{\pm} = \mp\omega T_1^{\pm} + R_1', \tag{42}$$

where

$$(A')_{ij} = A_{ij} + \sum_{l=1}^{m} \frac{B_{il}C_{lj}}{A_{ii} - D_{ll}}, \tag{43}$$

$$(R_1')_i = (R_1)_i + \sum_{l=1}^{m} \frac{B_{il}(R_2)_l}{A_{ii} - D_{ll}}, \tag{44}$$

and $i, j = 1, 2, \ldots, n$. The terms in Eqs. (42–44) come from single-particle excitations and their coupling with pair excitations, and this approximation scheme can be called PRA. The dimension of the matrix to be diagonalized in Eq. (42) is reduced to the dimension of single-excitation space. It is interesting to notice the modification of the denominators in Eqs. (43–44). Such necessity to change the energy denominators in a simplification procedure to include higher-order MBPT corrections was originally pointed out in Ref. [15]. Another simplification technique is to treat an ω-dependent matrix:

$$(A')_{ij} = A_{ij} + \sum_{l=1}^{m} \frac{B_{il}C_{lj}}{\mp\omega - D_{ll}}, \tag{45}$$

as suggested by Löwdin [16]. Such a partition technique has been recently applied by Geertsen, Rittby, and Bartlett [17] for the equation-of-motion CC method. Obviously, Eq. (43) is a further approximation of Eq. (45) and is easier to be implemented. Of course, the validity of the approximation should be tested by its numerical performance.

In a diagram representation, the terms in the left-hand side of Eq. (42) are shown in Fig. 1. In these diagrams, particles are denoted by upward lines and holes by downward lines. Dashed lines indicate interaction through the perturbation H_c. Exchange diagrams are also included but not pictured for simplicity. Double lines represent the correlation operator S, and bold lines the frequency-dependent correlation operator T. As a matter of fact, these bold lines represent effective interaction of the external field, and in the lowest order approximation they are simply the dipole interaction. Figure 1a accounts for final-state correlations. Contributions from Fig. 1b–c are called lowest-order core relaxation or rearrangement effects. The incoming core orbital represented by the free hole line in Fig. 1b and c is perturbed due to the excitation of core states, and then interacts with the outgoing virtual states. The diagrams of Fig. 1d–e are self-energy correction terms, where either the incoming or outgoing orbital excites core states and interact with the excitation. Particularly, when the incoming core orbital and the core state excited by the operator T are the same, Fig. 1d corresponds to the Δ(SCF) correction. Figure 1e can also be called polarization diagrams. The diagrams of Fig. 1f–i are another type of polarization diagrams. The external field excites a core state, then it interacts with the incoming orbital and the outgoing virtual states. The diagrams of Fig. 1j–l come from contributions of the coupled-cluster T_1S_2 terms, which are part of triple excitations. Figure 1j is usually called an RPA diagram appearing in the RPA

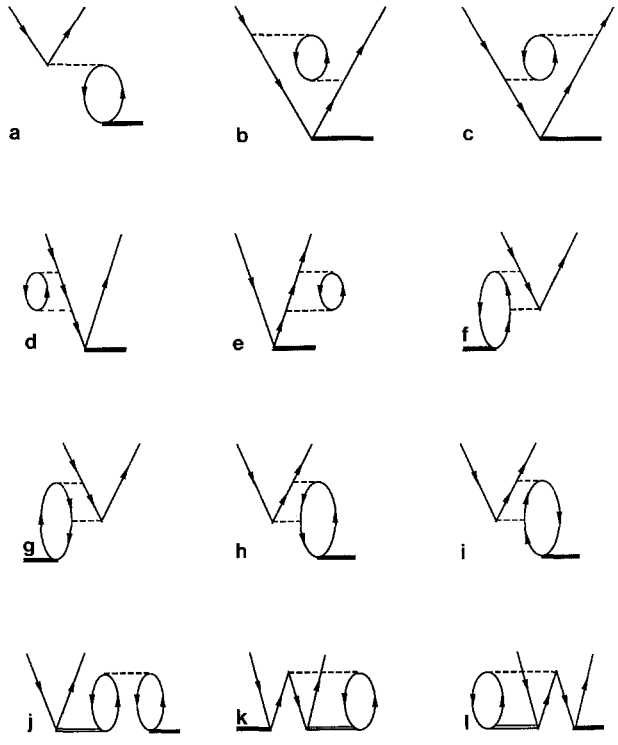

Fig. 1a–l. Diagrams contributing to the matrix A'. *Downward lines* denote core states/holes, upward excited states/particles. *Dashed lines* indicate electron-electron interaction. *Bold lines* represent the operator T, double lines the operator S

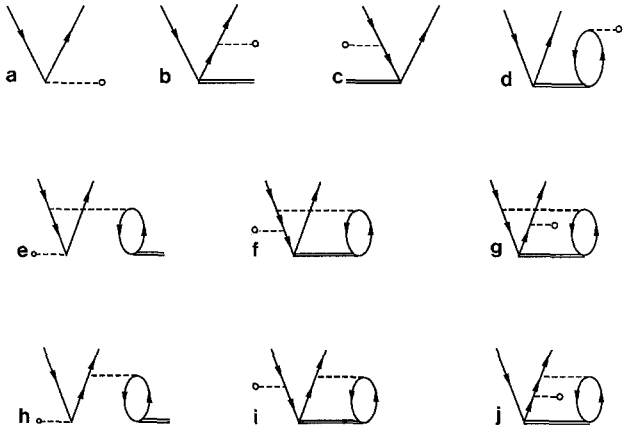

Fig. 2a–j. Diagrams contributing to the driving term R'_1. *Dashed lines with a circle* represent the external interaction

method. The diagrams of Fig. 1k–l give Brueckner-orbital-type corrections, and Fig. 11 can also be considered as an energy shift caused by the exclusion-principle-violation diagram [15].

The inhomogeneous driving terms of R' are shown in Fig. 2. Lines ending with a circle indicate the interaction of V'. Figure 2a is the lowest-order dipole term. Figure 2d is the ground-state correlation diagram. Other diagrams in Fig.

2 include higher-order ground-state correlation corrections for the dipole matrix element.

In solving Eqs. (42–44), instead of inverting the matrix in Eq. (42) for each frequency ω, we may first solve the homogeneous part of Eq. (42):

$$\sum_{(J)} A'_{(I)(J)} \langle (J) | i \rangle = \omega_i \langle (I) | i \rangle \tag{46}$$

with eigenvalues ω_i and eigenvectors $\langle (I) | i \rangle$, where the indices (I) and (J) stand for the indices (r, a) and (t, c) of the single-excitation amplitudes. Then, by inserting the Green's function:

$$G(\omega)^{\pm}_{(I)(J)} = \sum_i \frac{1}{\omega_i \pm \omega} \langle (I) | i \rangle \langle i | (J) \rangle \tag{47}$$

into Eq. (42), we are able to construct the required solution as:

$$T_1^{\pm} = G(\omega)^{\pm} R'_1. \tag{48}$$

Thus we deduce that $T_1^{\pm}$ has poles at all eigenfrequencies $\omega = \omega_i$ which correspond to excitation state energies of the system. Also, we can obtain oscillator strengths given by:

$$f_i = 2\omega_i \sum_{(I)(J)} (R_1)_{(I)} \langle (I) | i \rangle \langle i | (J) \rangle (R'_1)_{(J)}. \tag{49}$$

Consequently, the frequency-dependent polarizabilities are expressed as:

$$\alpha(\omega) = R_1 [G(\omega)^+ + G(\omega)^-] R'_1 = \sum_i \frac{f_i}{\omega_i^2 - \omega^2}. \tag{50}$$

The diagrams which contribute to $\alpha(\omega)$ are given in Fig. 3, where dashed lines with a solid dot represent the one-body dipole operator.

4. Numerical results for helium

We have used the present method to calculate the dynamic polarizabilities $\alpha(\omega)$ of He for frequencies up to beyond the $1s$-ionization threshold. An external dipole field induces two single-excitation channels $1s^2 \rightarrow 1snp(^3P)$ and (^1P), which are related to $p_{1/2}$ and $p_{3/2}$ channels in the jj coupling scheme. The numerical method used to solve the matrix Eq. (42) was based on the use of the finite basis sets described in Ref. [18]. Twenty-five positive energy states were generated from piecewise quartic polynomials. The calculation was carried out for angular momentum from 0 to 4 for the terms in Figs. 1–3. All virtual states were produced under the V_{HF}^{N-1}-type potential [19].

In Table 1 we compare the excitation energies, which are eigenvalues of Eq. (46), obtained by the present PRA method with relativistic TDS, RPA and experimental results. The TDA and RPA results were obtained from the present

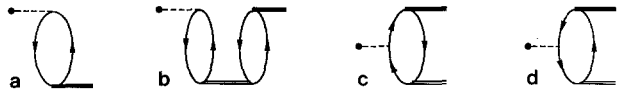

Fig. 3a–d. Diagrams contributing to $\alpha(\omega)$. *Dashed lines with a solid dot* represent the one-body dipole operator

Table 1. Triplet, singlet excitation energies (a.u.) and fine-structure splitting for He by TDA, RPA and the present method

Excited States	TDA[a]	RPA[b]	PRA[a]	Exp.[c]
$1s2p\ ^3P$	0.7804	0.780	0.7773	0.7704
$1s2p\ ^1P$	0.7972	0.797	0.7863	0.7797
$\Delta(2^1P\text{-}2^3P)$	0.0168	0.017	0.0090	0.0093
$1s3p\ ^3P$	0.8587	0.858	0.8541	0.8455
$1s3p\ ^1P$	0.8637	0.864	0.8570	0.8484
$\Delta(3^1p\text{-}3^3P)$	0.0050	0.005	0.0029	0.0029
$1s4p\ ^3P$	0.8852	0.885	0.8802	0.8712
$1s4p\ ^1P$	0.8873	0.887	0.8815	0.8725
$\Delta(4^1P\text{-}4^3P)$	0.0021	0.002	0.0013	0.0013
$1s5p\ ^3P$	0.8975	0.899	0.8924	0.8830
$1s5p\ ^1P$	0.8986	0.900	0.8931	0.8836
$\Delta(5^1P\text{-}5^3P)$	0.0011	0.001	0.007	0.0006

[a] From the present calculation
[b] Ref. [10]
[c] Ref. [20]

Table 2. Oscillator strengths for He calculated by TDA, RPA, the present PRA method, and compared with precise variational results

Transition	TDA[a]	RPA[b]	PRA[a]	"Accurate"[c]
$1s^2 \rightarrow 1s2p\ ^1P$	0.2602	0.252	0.2855	0.2762
$1s^2 \rightarrow 1s3p\ ^1P$	0.0731	0.070	0.0744	0.073
$1s^2 \rightarrow 1s4p\ ^1P$	0.0299	0.030	0.0296	0.030
$1s^2 \rightarrow 1s5p\ ^1P$	0.0168	0.024	0.0164	0.015

[a] From the present calculation
[b] Ref. [10]
[c] Ref. [21]

code which offers options to choose from different levels of approximations. Using finite basis sets to study dipole excitation in the RPA scheme has been reported by Johnson [10]. We used a smaller size of finite basis sets with 25 B-splines, and obtained essentially the same results. One interesting observation from Table 1 is the significant improvement of the calculated fine-structure splitting of singlet and triplet states of He in the present PRA method. This means that the relativistic PRA treatment yields a better balance between different channels of excited states.

Results of oscillator strengths for transitions from the ground state to the first four singlet states are listed in Table 2, and compared with TDA, RPA and variational-calculation results. The variational results were given by Schiff et al. [21] using highly accurate variational wave functions. Table 2 shows that the agreement between the present work and the accurate variational calculations is good.

Table 3. Frequency-dependent polarizabilities for He (a.u.) in length and velocity forms calculated by TDA, RPA, PRA, and compared with experimental results

ω	TDA[a]		RPA[a]		PRA[a]		Exp.[b]
	L	V	L	V	L	V	
0.0	1.398		1.322		1.389		1.383
0.1	1.413	1.314	1.336	1.336	1.404	1.329	1.399
0.2	1.459	1.357	1.380	1.380	1.453	1.375	1.449
0.3	1.545	1.437	1.463	1.463	1.545	1.462	1.542
0.4	1.689	1.572	1.600	1.600	1.699	1.608	1.700
0.5	1.932	1.799	1.834	1.834	1.965	1.860	1.973
0.6	2.392	2.229	2.275	2.275	2.484	2.350	2.502
0.7	3.591	3.353	3.433	3.433	3.968	3.952	3.884

[a] From the present calculation
[b] As fitted by Padé approximation [22]

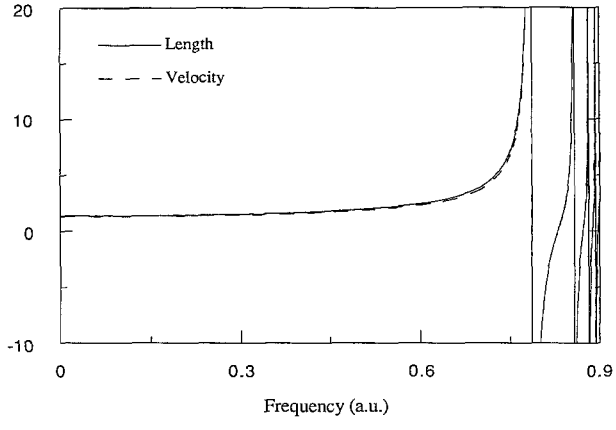

Fig. 4. Calculation of the dipole frequency-dependent polarizability $\alpha(\omega)$ of He below $1s$-ionization threshold. *Solid line* is the length result, *dashed line* the velocity result. The calculations are from the PRA method discussed in the text

In Table 3, we compare dynamic polarizabilities calculated by the TDA, RPA, PRA method with experimental results. The PRA results in the length form are in better agreement with experiment than the TDA and RPA method. Figure 4 illustrates the frequency-dependent polarizability for He in the length and velocity forms with ω below the photoionization threshold ω_1. The results in Fig. 4 were calculated using the PRA method. When ω is greater than ω_1, the denominator in $G(\omega)^-$ may vanish, and Eq. (50) should be modified as:

$$\alpha(\omega) = \sum_{\omega_j < \omega_1} \frac{f_j}{\omega_j^2 - \omega^2} + P \int_{\omega_1}^{\infty} \frac{df(\varepsilon)}{d\varepsilon} \frac{d\varepsilon}{\varepsilon^2 - \omega^2} + i \frac{\pi}{2\omega} \frac{df(\omega)}{d\omega}, \tag{51}$$

where P indicates principal-value integration and $df/d\omega$ is the differential oscillator strength distribution [23]. The real part of $\alpha(\omega)$ for He calculated by the PRA method is shown in Fig. 5.

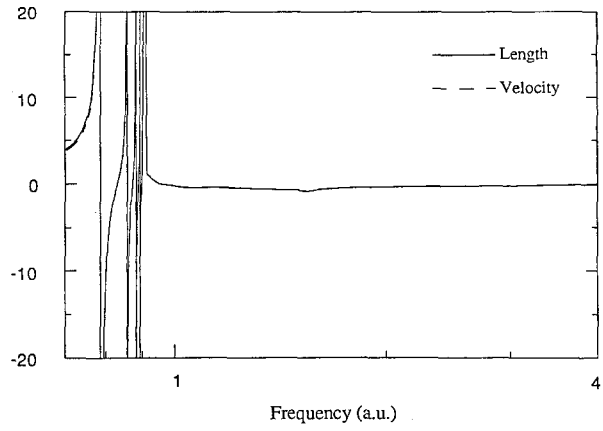

Fig. 5. Real part of $\alpha(\omega)$ for He. Length result indicated by *solid line*, velocity by *dashed line*

The imaginary part of $\alpha(\omega)$ in Eq. (51) leads to photoionization and is related to the cross section by the equation [24]:

$$\sigma(\omega) = \frac{4\pi}{c}\,\omega\ \mathrm{Im}\,\alpha(\omega). \tag{52}$$

The present procedure provides a useful alternative for molecular photoionization calculations, since it does not require continuum orbitals which are difficult to obtain for multicenter systems. One indirect algebraic approach to extract photoionization cross section is the Stieltjes-integral approximation developed by Langhoff et al. [23]. Another approach, suggested by Veseth [25], is to use the relation:

$$\alpha(i\eta) = \frac{c}{2\pi^2}\int_0^\infty \frac{\sigma(\omega)}{\eta^2+\omega^2}\,d\omega \tag{53}$$

to derive $\sigma(\omega)$ from values of $\alpha(i\eta)$. Implementation of the approach based on Eq. (53) is in progress.

In summary, the PRA method provides an effective approximation in applying time-dependent coupled-cluster theory (TDCC) to atomic and molecular dynamic processes. Higher-order correlation effects are included, and numerical results for excitation energies, oscillator strengths and frequency-dependent polarizabilities for the He calculations of this paper are encouraging. The present method can also be extended to calculate photoionization cross sections.

Acknowledgements. We would like to thank the organizers of the Workshop on Coupled Cluster Theory at the Interface of Atomic Physics and Quantum Chemistry, Aug. 1990. Financial support from the National Science Foundation, NSF Grant No. PHY-89-07258, is acknowledged. This work is supported by NSF Grant No. PHY 90-07883. It is a pleasure to thank Dr. L. Veseth for providing preprints of his work prior to publication.

References

1. Monkhorst HJ (1977) Int Quantum Chem Symp 11:421
2. Mukherjee D, Mukherjee PK (1979) Chem Phys 39:325
3. Sekino H, Bartlett RJ (1984) Int Quantum Chem Symp 18:255

4. Dalgaard E, Monkhorst JH (1983) Phys Rev A 28:1217
5. Cizek J (1966) J Chem Phys 45:4246; (1969) Adv Chem Phys 14:35
6. Lindgren I (1974) J Phys B 7:2441; (1978) Int Quantum Chem Symp 12:33
7. Bartlett RJ (1981) Ann Rev Phys Chem 32:359
8. For example, see Fetter A and Walecka JD (1971) Quantum theory of many-particle systems. McGraw-Hill, New York
9. Amusia MYa, Cherepko NA (1975) Case Studies in Atomic Physics 5:49
10. Johnson WR (1988) Adv At Mol Phys 25:375
11. Akhiezer AI, Berestetskii VB (1965) Quantum electrodynamics. Interscience, New York
12. Blundell SA, Johnson WR, Liu ZW, Sapirstein J (1989) Phys Rev A 40:2233
13. Miller TM, Bederson B (1977) Adv At Mol Phys 13:1
14. See the review by Oddershede J (1978) Adv Quantum Chem 11:275
15. Kelly HP (1969) Adv Chem Phys 14:129
16. Löwdin PO (1963) J Mol Spectr 10:12
17. Geertsen J, Rittby M, Bartlett RJ (1989) Chem Phys Lett 164:57
18. Johnson WR, Sapirstein J (1986) Phys Rev Lett 57:1126; Johnson WR, Blundell SA, Sapirstein J (1988) Phys Rev A 37:307
19. Silverstone HJ, Yin ML (1968) J Chem Phys 49:2026; Huzinaga S, Arnau C (197770) Phys Rev A 1:1285
20. Moore CE (1971) Atomic Energy Levels, NBS (U.S.) Circ No 35, U.S. GPO, Washington D.C.
21. Schiff B, Pekeris CL, Accad Y (1971) Phys Rev A 4:885
22. Langhoff PW, Karplus M (1969) J Opt Soc Am 59:863
23. Langhoff PW, Sims J, Corcoran CT (1974) Phys Rev A 10:839; Langhoff PW, Corcoran CT (1974) J Chem Phys 61:146
24. Fano U, Cooper JW (1968) Rev Mod Phys 40:441
25. Veseth L (1991) Phys Rev A 44:358